Assessing Future Changes in the East Asian Summer Monsoon Using CMIP3 Models: Results from the Best Model Ensemble

KYONG-HWAN SEO AND JUNG OK

Department of Atmospheric Sciences, Division of Earth Environmental System, Pusan National University, Busan, South Korea

(Manuscript received 9 February 2012, in final form 13 September 2012)

ABSTRACT

Future changes in the East Asian summer monsoon (EASM) have been estimated from the six best-performing models in phase 3 of the Coupled Model Intercomparison Project (CMIP3) included in the Fourth Assessment Report (AR4) of the Intergovernmental Panel on Climate Change (IPCC). The composite mean rainband over East Asia during the summer season exhibits the characteristic EASM front relatively well with slightly less precipitation over east–central China and the baiu front aligned more steeply in the latitudinal direction. An ensemble from the coupled models that poorly simulated the EASM is shown to degrade the overall results, giving rise to an underestimation of the projected increase rate in precipitation. In a quantitative estimate, the 22-member ensemble-mean precipitation for the period 2079–99 is anticipated to increase by only 5%–10%, which is half the increase in the corresponding mean precipitation from the good models (10%–20%). Moisture budget analysis demonstrates that the good-model ensemble mean is in a much closer correspondence with observations than the poor- or all-model ensemble mean, supporting the reliable selection of the best-performing models. An increase in the vertically integrated moisture flux convergence is attributed to the enhanced precipitation in the future climate. In particular, a significant increase in atmospheric water vapor because of a warmer SST over the western Pacific plays a more critical role in the enhanced precipitation than a change in monsoonal low-level circulation does. In contrast to the apparent meridional shift of the primary location of the future EASM front presented in previous studies, the current analysis shows a negligible amount of meridional movement.

1. Introduction

East Asian summer monsoon (EASM) projections for future climate changes, determined using phase 3 of the Coupled Model Intercomparison Project (CMIP3) models, have been investigated in many previous studies (e.g., Kitoh and Uchiyama 2006; Min et al. 2006; Zhou and Yu 2006; Kripalani et al. 2007; Lu et al. 2007; Chen and Sun 2009; Lu and Fu 2010; Kusunoki et al. 2011; Kusunoki and Arakawa 2012). The monsoonal rainfall in the entire East Asian region is expected to intensify owing to global warming. For example, Min et al. (2006) showed that the precipitation increase over East Asia in the twenty-first century (21C) would be greater than the increase in the global-mean precipitation. Kripalani et al. (2007) demonstrated an ~8% increase in precipitation over Korea, Japan, and central and northern China. This increase is mainly attributed to enhanced moist southerly flows over coastal East Asia (Lu et al. 2007). However, most previous approaches to assessing future changes in the EASM under global warming scenarios analyze either one specific model or a grand ensemble from all available models and thus are subject to uncertainties created through various interpretations, depending on the choice of models or datasets. Therefore, selection of the climate models that simulate the EASM realistically is required prior to assessment to determine the ensemble mean using only best-performing model outputs.

The objective of the present study is to select the best-performing models and to predict the future changes in the EASM with enhanced credibility using 22 CMIP3 models introduced in the Intergovernmental Panel on Climate Change (IPCC) Fourth Assessment Report (AR4). These models are compared with an all-member ensemble and ensembles from poorly performing models. The current analysis technique, simple but very effective,

Corresponding author address: Dr. Kyong-Hwan Seo, Department of Atmospheric Sciences, Pusan National University, Busan 609735, South Korea.
E-mail: khseo@pusan.ac.kr

DOI: 10.1175/JCLI-D-12-00109.1

© 2013 American Meteorological Society

TABLE 1. Acronyms for the 22 CMIP3 models and their expansions.

Model	Expansion
BCM2	Bergen Climate Model, version 2
CCSM3	Community Climate System Model, version 3
CNRM-CM3	Centre National de Recherches Météorologiques Coupled Global Climate Model, version 3
CSIRO MK 3.0	Commonwealth Scientific and Industrial Research Organisation Mark, version 3.0
ECHAM5	—
ECHO-G	ECHAM and the global Hamburg Ocean Primitive Equation
FGOALS-g1.0	Flexible Global Ocean–Atmosphere–Land System Model gridpoint, version 1.0
GFDL CM2.0	Geophysical Fluid Dynamics Laboratory Climate Model, version 2.0
GFDL CM2.1	Geophysical Fluid Dynamics Laboratory Climate Model, version 2.1
GISS-AOM	Goddard Institute for Space Studies, Atmosphere–Ocean Model
GISS-EH	Goddard Institute for Space Studies Model E-H
GISS-ER	Goddard Institute for Space Studies Model E-R
HadCM3	third climate configuration of the Met Office Unified Model
HadGEM	Hadley Centre Global Environmental Model, version 1
INM-CM3	Institute of Numerical Mathematics Coupled Model, version 3
IPSL CM4	L'Institut Pierre-Simon Laplace Coupled Model, version 4
MIROC3.2(hires)	Model for Interdisciplinary Research on Climate, version 3.2, high-resolution
MIROC3.2(medres)	Model for Interdisciplinary Research on Climate, version 3.2, medium-resolution
MRI CGCM2.3.2	Meteorological Research Institute Coupled General Circulation Model, version 2.3.2
MRI CGCM3.1 T47	Meteorological Research Institute Coupled General Circulation Model, version 3.1, T47 resolution
MRI CGCM3.1 T63	Meteorological Research Institute Coupled General Circulation Model, version 3.1, T63 resolution
PCM1	Parallel Climate Model, version 1

will provide better assessment of EASM change in the future climate.

2. Datasets and methods

Primary observational datasets include that from the Climate Prediction Center (CPC) Merged Analysis of Precipitation (CMAP; Xie and Arkin 1997) and the National Centers for Environmental Prediction/Department of Energy (NCEP/DOE) Reanalysis-2 (Kanamitsu et al. 2002). For the model data, we used the World Climate Research Programme (WCRP) CMIP3 multimodel datasets collected and archived by the Program for Climate Model Diagnosis and Intercomparison. The list and properties of the 22 atmosphere–ocean coupled general circulation models (AOGCMs) are found online (http://www-pcmdi.llnl.gov/ipcc/model_documentation/ipcc_model_documentation.php).

Each dataset differs in horizontal grid points and time intervals; therefore, for ease of comparison, the datasets are interpolated into a 2.5° × 2.5° horizontal grid for 21-yr periods from 1979 to 1999 using a bilinear interpolation method and are then compared with observational results. Future climate data are also prepared for 21-yr periods of 2079–99 using the Special Report on Emissions Scenarios (SRES) A1B simulations. The domain of the East Asian region is defined as 20°–50°N and 100°–180°E. All analyses are conducted for the boreal summer season [June–August (JJA)]. All variables used in this study are monthly-mean data.

Summertime-mean precipitation from simulations of CMIP3 models over the EASM region is evaluated for the current climate (1979–99) to select the best models. Climatological-mean and interannual standard deviation distributions are compared with observations using a Taylor diagram (Taylor 2001), which provides a concise statistical summary of the degree of correlation, root-mean-square difference, and variance ratio. Only models selected through this procedure are used to determine the best future projections of the EASM.

3. Model performance

a. Classification of the 22 AOGCMs

It has been recognized that poorly selected models degrade the overall skill of weather and climate forecasts in an ensemble-mean approach (Krishnamurti et al. 2000). To distinguish good and poor models from the 22 CMIP3 models (model expansions provided in Table 1), two Taylor diagrams are used on the basis of the composites of climatological-mean field (Fig. 1a) and interannual standard deviation field (Fig. 1b) for summer-mean precipitation in the EASM region. Since mean and variance explain much of the basic features inherent in climate variability, the first two moment statistics are used. The following three criteria are applied to select highly or poorly performing models: 1) the pattern correlation (i.e., the cosine of the azimuthal angle in a polar coordinate in the figure) in the

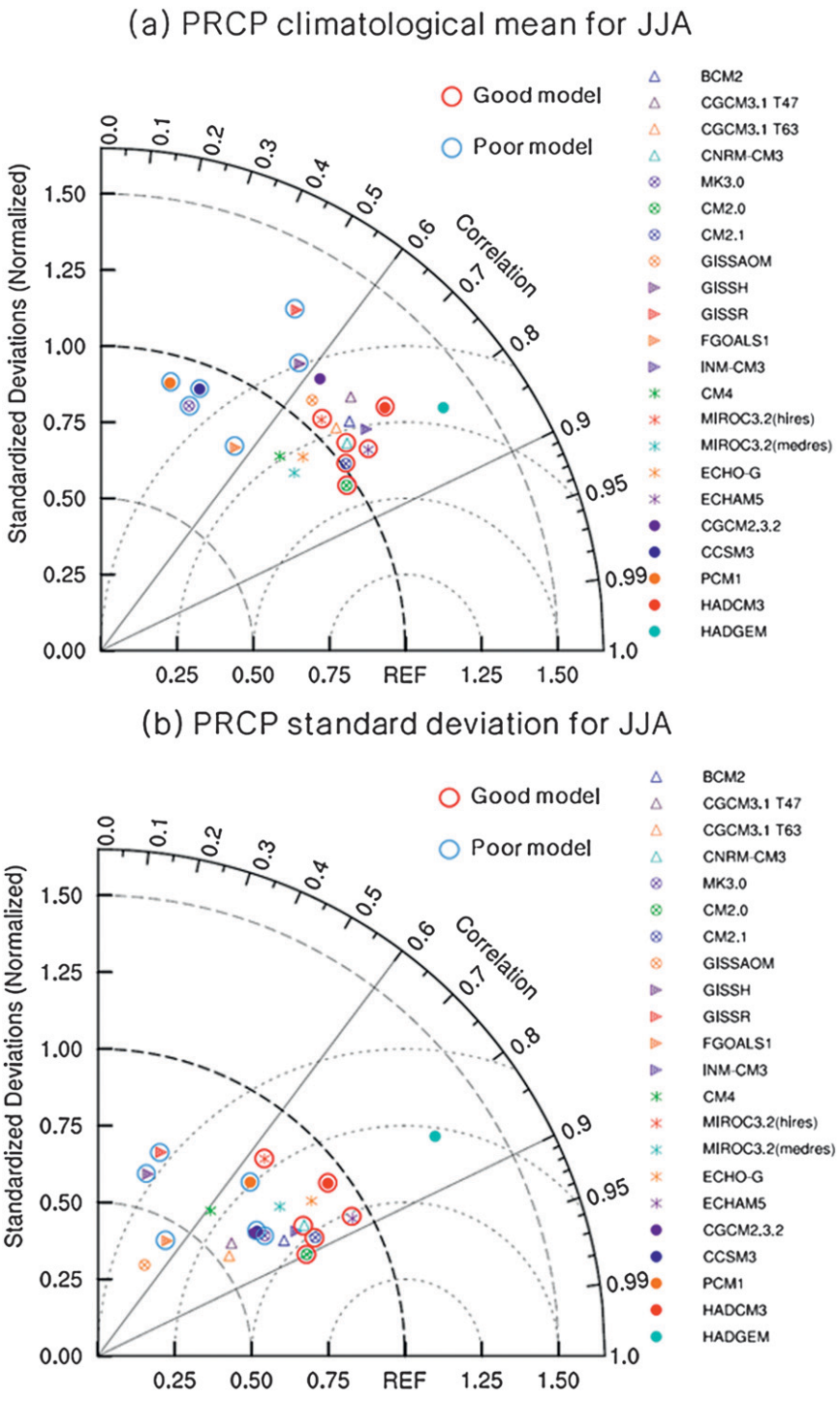

FIG. 1. Taylor diagram analysis of JJA-mean precipitation over the EASM region during the period of 1979–99 for 22 AOGCMs. (a) Provides the composites of climatological-mean field and (b) gives the interannual standard deviation field.

climatological-mean field (Fig. 1a) should be greater (less) than 0.6 for a good (poor) model; 2) in the interannual standard deviation field (Fig. 1b), the pattern correlation should be greater than 0.6 and the spatial standardized deviation ratio (the spatial standard deviation normalized by the observed spatial standard deviation) should be within the range of 1.00 ± 0.25 for a good model; 3) in the interannual standard deviation

field (Fig. 1b), the spatial standardized deviation ratio should be outside of 1.00 ± 0.25 for a poor model. Note that these criteria tend to put more weights on the correlation skill in the climatological-mean field.

According to the above criteria, six each of highly and poorly performing models, represented in both figures by red and blue open circles, respectively, are selected. The good models include ECHAM5, CNRM-CM3, MIROC3.2(hires), GFDL CM2.1, GFDL CM2.0, and HadCM3; poor models include CSIRO MK 3.0, GISS-ER, GISS-EH, PCM1, FGOALS-g1.0, and CCSM3. The ECHO-G model is categorized as a good model, but future climate data are not available so it is excluded in the calculation of further statistics. Also, although HadGEM shows relatively similar pattern correlations in the seasonal mean and interannual standard deviation of precipitation as those of the good models, it is not selected because the spatial standard deviation ratio (ordinate in Fig. 1a) is excessively high. This large spatial standard deviation ratio is related to a wet model bias. A previous study showed that this model had the largest wet bias in summer precipitation over the East Asian region among the 23 CMIP3 models participating in AR4 (Kim et al. 2008). Most of the selected good models exhibit the spatial standardized deviation ratios located closer to unity (reference line) than the poor models do. Note that a posterior sensitivity test shows that addition/exclusion of one or two models in the ensemble model groups does not affect the main conclusions drawn in this study. Temporal variation information, such as a trend, is not used as one of selection criteria because to some extent, all climate models tend to underestimate the observed increasing trend of precipitation.

b. Present-day climate simulations

Figure 2 shows the summer-mean precipitation, 850-hPa moisture flux and its magnitude, and surface air temperature for observation and ensembles of the 22 models, the good models, and the poor models. In Fig. 2a, the observed pattern of precipitation is characterized by a prominent rainband associated with the mei-yu–hangma–baiu front from the southeastern part of China through the Korean Peninsula to Japan. Meanwhile, the 22-AOGCM ensemble mean shows lower rainfall intensity over the major band, as similarly shown in Kripalani et al. (2007). On the contrary, the good-model ensemble mean captures the intensity and pattern of the major rainband more realistically. The poor-model ensemble-mean rainfall shows a stronger underestimation than that of the good- and 22-member ensembles. It should be noted, however, that even the good-model ensemble mean shows less precipitation over the East Asian region than the observation, corresponding to a degeneracy of dry bias present in the contemporary AOGCMs.

Figure 2b shows the patterns of 850-hPa moisture flux vector ($q\mathbf{V}_H$, where q and $\mathbf{V}_H$ are specific humidity and horizontal wind vector, respectively) and its magnitude: the intensity and direction of which are effectively simulated by the good-model ensemble mean, especially in southern Japan; other ensemble means underestimate the moisture transport from the northern South China Sea. This deficiency is closely related to a weaker intensity in simulated precipitation, shown in Fig. 2a. Figure 2c shows the composite surface air temperature fields. The basic seasonal pattern of surface air temperature, in which the land is significantly warmer than the ocean, is relatively well reproduced by each of the three ensemble means; however, the good ensemble mean showed excellent reproducibility in east China (Fig. 2c). In addition to the moisture flux and surface air temperature, structures and intensities of sea level pressure and upper-level jet stream are also better represented in the good-model ensemble (not shown) than in other ensemble groups. Therefore, it is of interest to note that, even if the selection of good models is based solely on precipitation, other thermodynamic and dynamic fields composited from the good models all show much more realistic spatial patterns than those of the 22-member or poor-model ensemble mean.

4. Results of future climate simulations

Future precipitation projections over East Asia for each ensemble group under the IPCC A1B scenario are presented in Fig. 3. Two important issues related to changes in precipitation intensity and location are mainly examined for the 21-yr period 2079–99. It is evident that the pattern of the East Asian precipitation under the global warming scenario (Fig. 3a) is similar to present-day climate patterns (Fig. 2a); however, the magnitude of the major rainband along the EASM front is strengthened, as discussed in previous studies (e.g., Min et al. 2004; Kimoto et al. 2005; Min and Jhun 2010). The difference field between present and future climate (not shown) demonstrates a prominent increase in precipitation mainly along the changma–baiu front. In relation to mei-yu, enhanced rainfall occurs over south China and Taiwan, whereas a very slight decrease in precipitation is observed in the central China. Predictions based on the good-model ensemble include a statistically significant increase of precipitation by about 10%–20% over the major rainband region (Fig. 3b), whereas an increase rate in the all-member ensemble precipitation is 5%–10% with the statistically significant area concentrated only over the North Pacific Ocean (Fig. 3c). Kusunoki

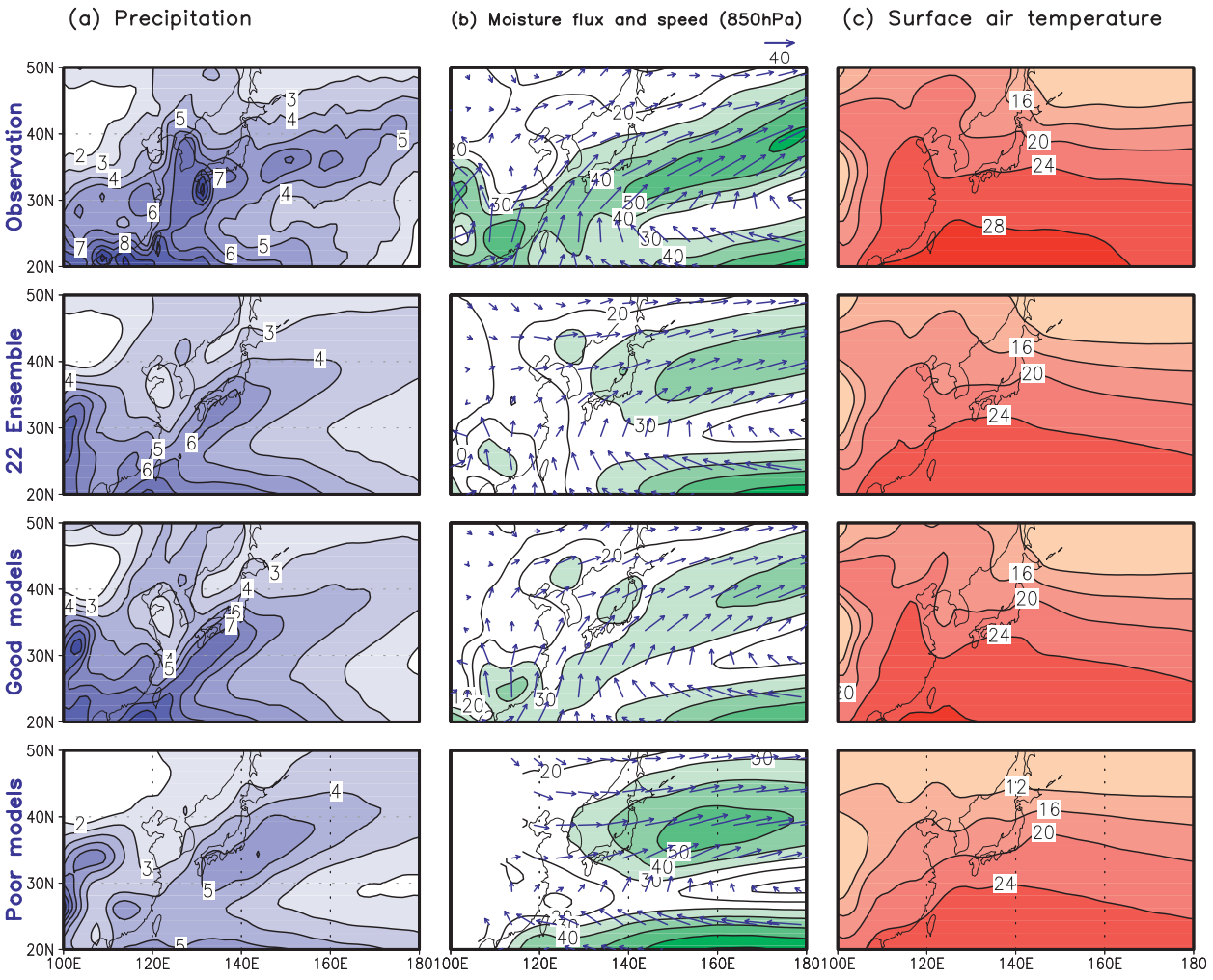

FIG. 2. Distribution of JJA-mean (a) precipitation (mm day^{-1}), (b) moisture flux (vector) and its magnitude (shading) at 850 hPa (g kg^{-1} m s^{-1}), and (c) surface air temperature (°C) over the EASM region for the present climate conditions (1979–99) for observation and 22-model, good-model, and poor-model ensemble means.

and Arakawa (2012) have investigated future changes in June–July precipitation intensity using CMIP3 simulations (their Fig. 7d). The overall pattern of precipitation changes is very similar to this study with an increase of precipitation over most of the EASM region, except for central China, where precipitation is projected to decrease. In particular, in both studies, the local peak areas in precipitation increase greater than 20% are seen over the Yellow Sea west of the Korean Peninsula and the Japan Sea south of Kuril Islands. However, over the baiu region (25°–35°N), our increase rate in the future is greater than their result by more than 5%. This discrepancy may be because of the different selection of models and analysis period used. On the other hand, the poor-model ensemble (Fig. 3d) shows a very different increase pattern than the good-model ensemble. The largest increase rate is located south of the major frontal band and the statistical significant region appears over the North Pacific.

Therefore, the increase rate in precipitation projected from the good models is twice greater than that from the 22-member ensemble over the main frontal band. We will show later using moisture budget analysis how similar or dissimilar the selected model groups are relative to observation.

The pattern of cumulus convective precipitation under global warming is similar to that of the total precipitation (Fig. 3e), and it amounts to approximately 50% of the total summer precipitation in the EASM region. The cumulus convective precipitation from the good-model ensemble suggests an increase of 10%–30% over the major monsoonal rainband and of 50% near Korea and its neighboring western sea (Fig. 3f). Note that the projected increase in the convective precipitation

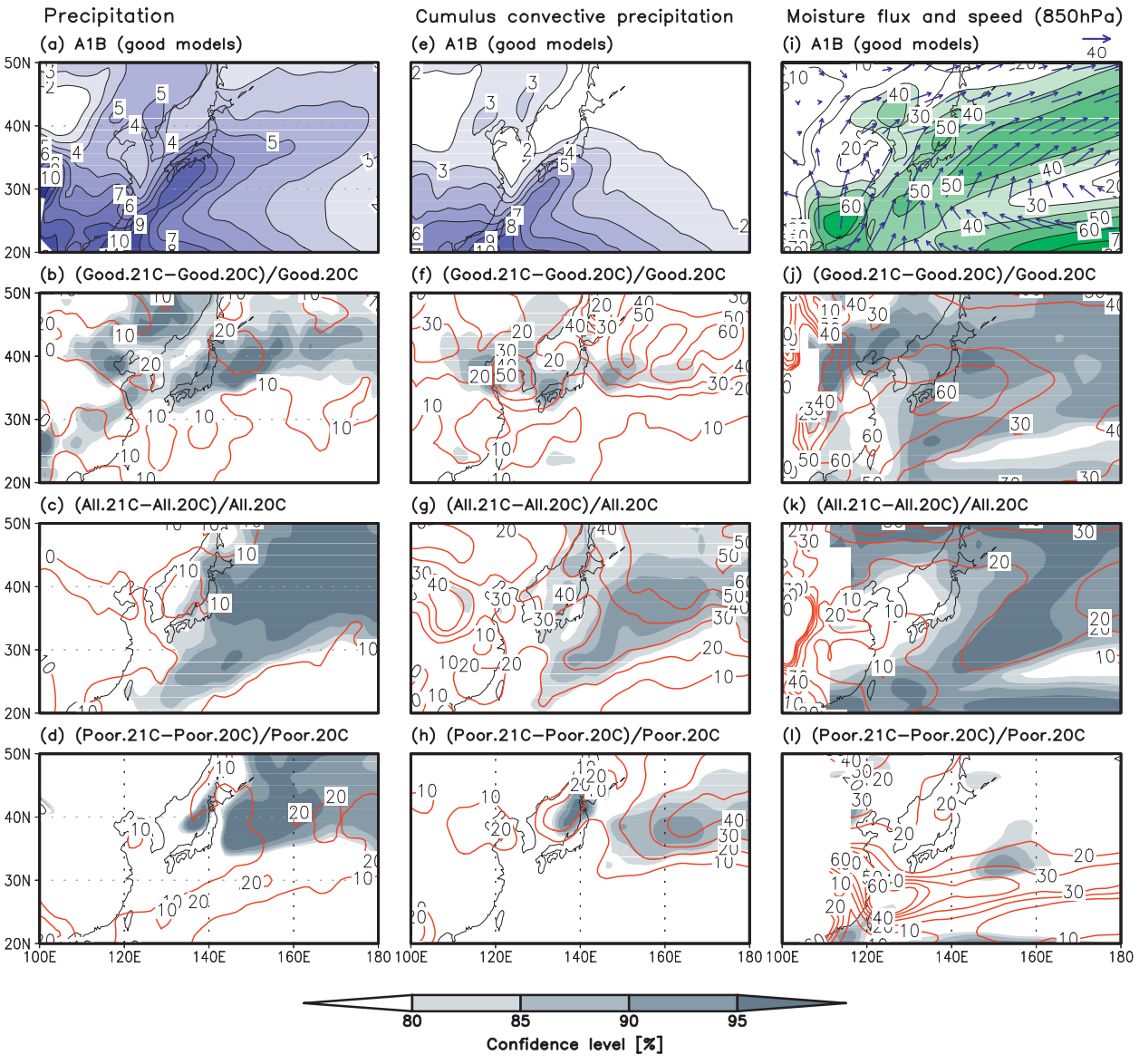

FIG. 3. Distribution of JJA-mean total precipitation (mm day^{-1}), cumulus convective precipitation (mm day^{-1}), and moisture flux and its magnitude at 850 hPa (g kg^{-1} m s^{-1}) for the period of 2079–99 under the A1B scenario. (a),(e),(i) Spatial patterns of future precipitation from the good-model ensemble; (b),(f),(j) fractional increase rates (%) for the good-model ensemble; (c),(g),(k) fractional increase rates (%) for the all-member ensemble; and (d),(h),(l) fractional increase rates (%) for the poor-model ensemble. The red line is an increase rate and gray shading denotes the confidence level. Student's *t* test is used.

over the central North Pacific is as high as 20%–50%, but this region generally attains only a small convective precipitation amount, limiting the significance of this increase rate. A comparison with Fig. 3b demonstrates that the cumulus convective precipitation increase is significantly greater than the total precipitation, implying that the change in the total precipitation is mainly due to the enhancement of cumulus convective activity (Min and Jhun 2010). Except for a moderately lower increase rate, the all-member ensemble-mean patterns are essentially similar to those of the good-model ensemble (Fig. 3g). An increase in the poor-model ensemble mean appears outside of the main monsoonal rainband (Fig. 3h).

Moisture flux over the EASM domain from the good models is also projected to significantly intensify in the future (Fig. 3i), with a maximum increase rate of 60% over the present climate along the major rainband (Fig. 3j). However, the all-member ensemble mean shows only a 10%–20% increase rate (Fig. 3k). The moisture

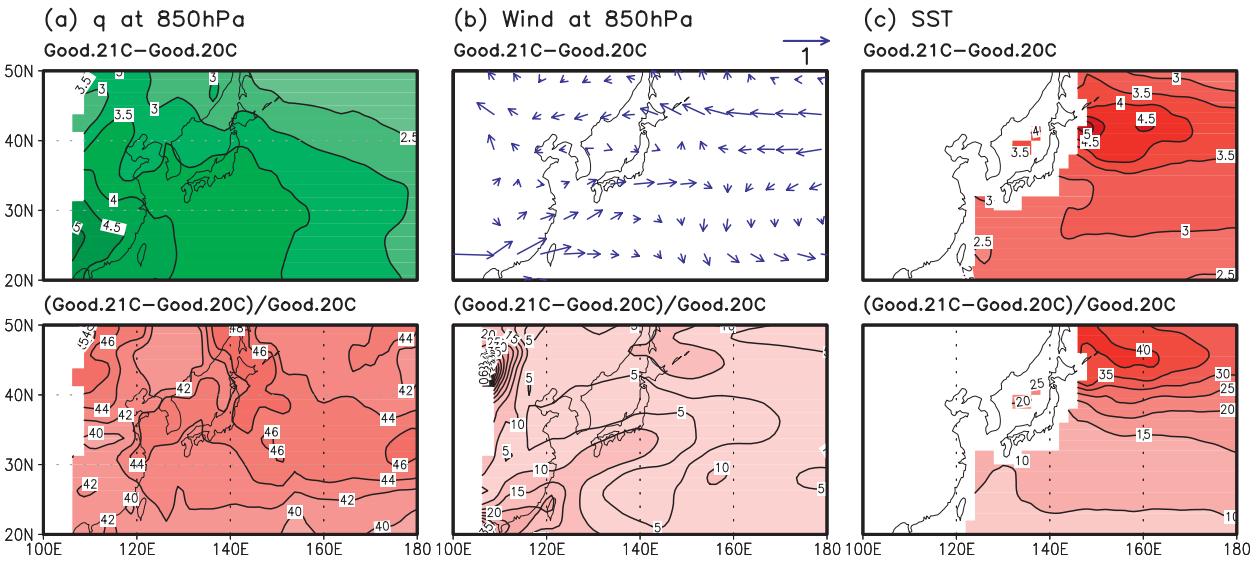

FIG. 4. Future changes in JJA-mean (a) specific humidity at 850 hPa (g kg^{-1}), (b) horizontal wind at 850 hPa (m s^{-1}), and (c) sea surface temperature (°C) for the good-model ensemble mean. (top) The future change (21C − 20C) and (bottom) the fractional change rates [(21C − 20C)/20C] (%) relative to the present-day climate.

flux in the poor-model ensemble is statistically insignificant (Fig. 3l). Therefore, the moisture flux in the good model is 30%–50% more than that suggested by the 22-member mean. Thus, the use of an all-member ensemble mean or grand multimodel ensemble mean without prior determination of nicely and poorly performing models tends to underestimate the strength of precipitation, particularly convective precipitation and low-level moisture flux.

One of the most crucial factors for enhanced precipitation in the future is considered the enhanced moisture flux $q\mathbf{V}_H$ seen in Fig. 3i. To investigate the relative importance, the future changes in q and $\mathbf{V}_H$ are computed. Figure 4 shows differences in specific humidity and wind magnitude between the future and present climate (top panels). Their fractional percentage increase rates relative to the present climate are shown in the bottom panels. As can be seen in water vapor (Fig. 4a), a more than 40% increase is evident in the future climate relative to the present-day climate. The increase occurred in the whole domain is statistically significant at 1%. This increase of water vapor is primarily due to a ~2.5°–4°C increase in the SST over the vast western Pacific, including the EASM region under the warm climate (Fig. 4c). By contrast, low-level horizontal winds are simulated to increase in the future only by less than 10% (Fig. 4b), which is not statistically significant at a level of even 15%. This insignificant change in the strength of horizontal winds is consistent with a negligible change in sea level pressure over the EASM region (not shown). Therefore, the robust feature of the strengthened moisture flux in Fig. 3i results mainly from an increase in the amount of atmospheric water vapor in the warm environment not from the slightly strengthened southwesterlies.

One may ask if the precipitation change projected by the good-model ensemble is statistically different from that by the poor-model ensemble or all-model ensemble. Figure 5a shows the difference between the future changes in precipitation estimated from the good-model ensemble and poor-model ensemble. Shading denotes the significant region at levels of 5% and 10% estimated using Student's t test. As can be seen, the difference occurs mainly along the major rainband with the future precipitation increase from the good-model ensemble statistically different from that of the poor-model ensemble. A comparison with the future change from the all-model ensemble (Fig. 5b) shows much reduced difference between the two model groups since the good-model results are also used for the all-model ensemble; however, it still shows a statistically significant difference. Therefore, our selection of the good models is proven very reliable and provides statistically meaningful differences in the estimation of the future precipitation change.

To estimate important processes for the production of precipitation along the monsoon front in a more quantitative manner, the water vapor budget equation is analyzed (i.e., Yoon and Chen 2005; Hsu et al. 2012; Seager et al. 2010). This also provides a useful insight as to why the selected good models outperform the rest of models over the EASM region. The moisture budget is

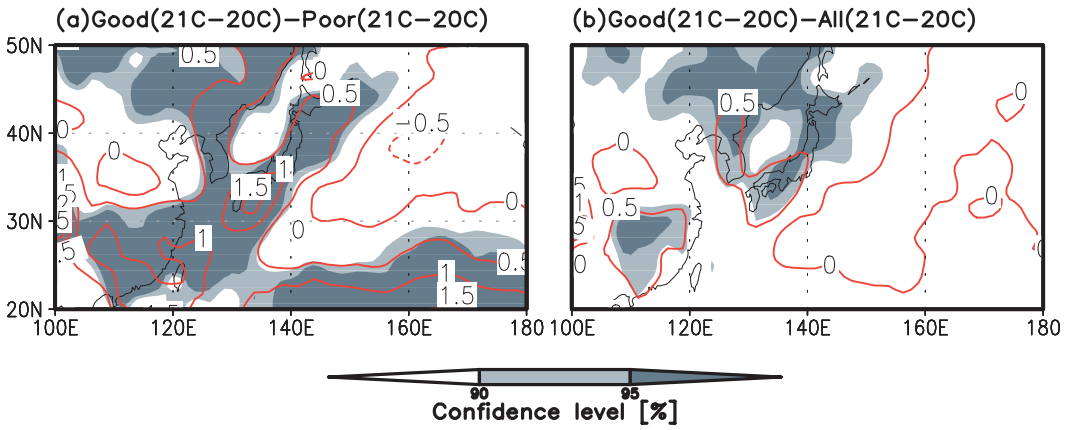

FIG. 5. Statistical significance test of JJA-mean precipitation (mm day^{-1}) for (a) the difference between good-model ensemble change (21C − 20C) and poor-model ensemble change (21C − 20C) and (b) the difference between good-model ensemble change (21C − 20C) and all-model ensemble change (21C − 20C). The red line is the difference between ensemble groups and gray shading denotes the confidence level. Student's *t* test is used.

calculated as follows for the region of the major monsoonal rainband (26°–46°N, 114°–151°E):

$$\frac{\partial w}{\partial t} + \langle \nabla \cdot (q\mathbf{V}_H) \rangle = E - P + \text{Res}, \qquad (1)$$

where w is precipitable water (total column water vapor), $\langle\,\rangle$ denotes a vertical integration from 1000 to 100 hPa, P is precipitation, and E is evaporation from the surface, and Res is residual. The residual includes computational errors, submonthly contributions, biases in the data assimilation system, and inconsistency between the NCEP/DOE reanalysis and CMAP data. The time rate of change of water content is calculated by the centered finite difference scheme. The second term in (1) can be further broken up into contributions from horizontal dry advection $\mathbf{V}_H \cdot \nabla q$ and moisture divergence associated with mass divergence $q\nabla \cdot \mathbf{V}_H$. Figure 6 shows the estimated values of each term for the observation and good, poor, and all-model ensemble means. The most prominent features of the moisture budget analysis are summarized:

1) The individual terms of (1) for the good-model ensemble mean are most similar (even though slightly underestimated) to those of the observation, supporting the credible selection of the best-performing models.
2) The poor-model ensemble mean has the largest differences with the observation. While the observation and other ensemble groups show moist advection, this ensemble mean shows an opposite sign and moisture divergence is too small. In addition, it shows overly strong evaporation. Representation of moisture flux convergence and evaporation in the model is problematic, giving rise to much less precipitation.
3) Therefore, a projected change in precipitation in future climate estimated from the selected good models is more reliable than that from the poorly performing models or all-member ensemble mean.
4) Among the two components that comprise moisture flux convergence $-\nabla \cdot q\mathbf{V}_H$ (which produces rainfall along the monsoon front), positive moisture advection $-\mathbf{V}_H \cdot \nabla q$ is greater than moisture convergence associated with mass convergence $-q\nabla \cdot \mathbf{V}_H$ by about 20%–30% in both the observation and the good-model ensemble mean. However, the moisture convergence is expected to increase about twice more than the moisture advection in the future climate. This is because of a strong increase in the amount of water vapor (by more than 40%) from an enhanced evaporation in the warm climate not to the slightly increased southwesterlies or their convergence as shown in Fig. 4.

Along with these results, the statistically significant differences between the good-model ensemble and the poor-model ensemble or all-model ensemble (shown in Fig. 5) explain why the good-model ensemble estimates a more enhanced rainfall in the EASM region in the future with sufficient credibility than the poor-model ensemble or all-model ensemble does.

Previous studies demonstrated an apparent meridional movement of the monsoonal band and particularly a northward shift of the monsoonal convergence zone in the future (e.g., Min et al. 2004; Kimoto 2005). In contrast, Li et al. (2010) used 14 AOGCMs to show a southward shift of the EASM-related major circulation components in a warming climate. On the basis of

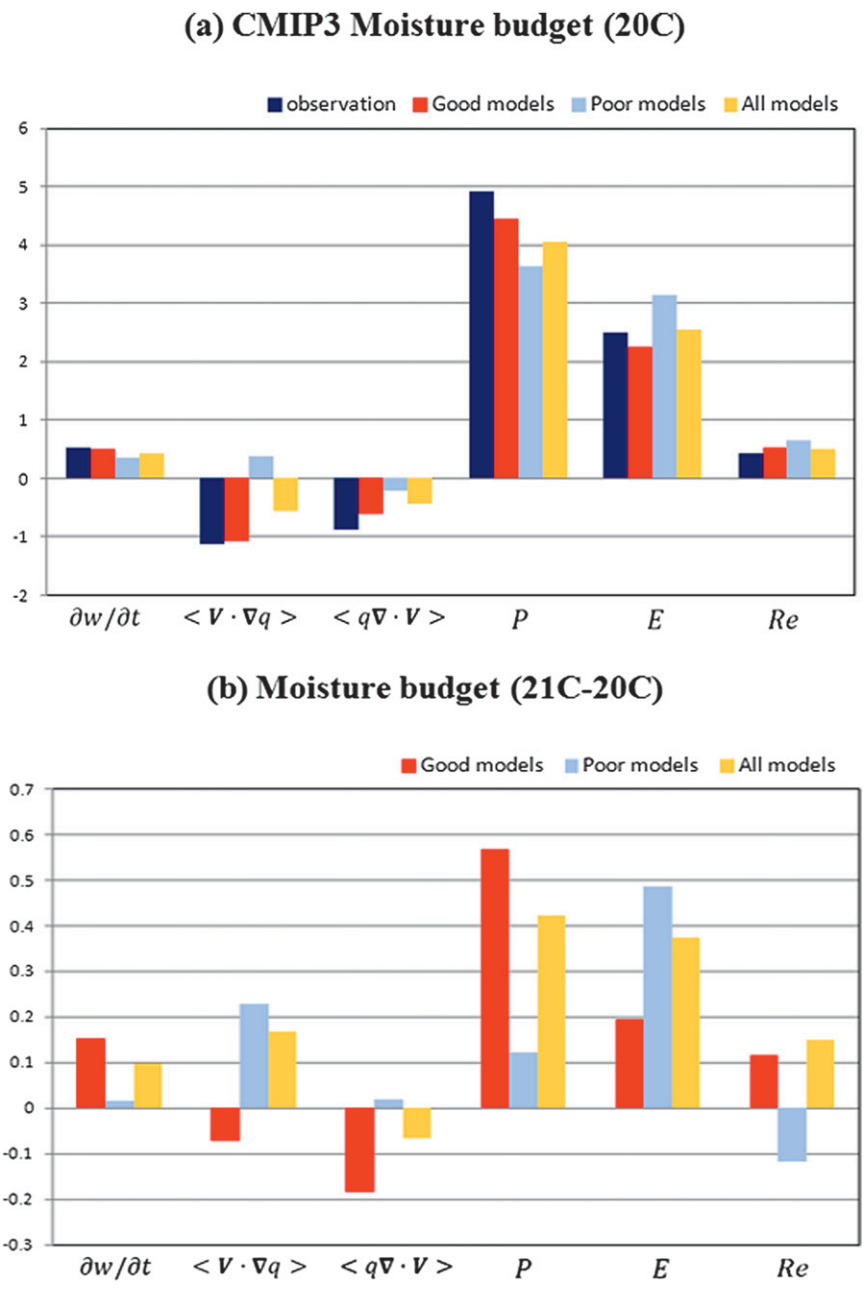

FIG. 6. JJA-mean moisture budget for (a) the present-day climate (20C) and (b) future change (21C − 20C) for observation and good-model, poor-model, and all-model ensemble means over the major rainband region. All units are millimeters per day.

this southward shift, precipitation in the northern part of the Korean Peninsula is projected to decrease in the 20-km mesh atmospheric GCM simulation (Yun et al. 2008). In the current study, we examine the possible meridional shift of the monsoon front using the selected good models and estimate the major frontal band by connecting the local maximum precipitation intensities for these models only. As shown in Fig. 7, the major rainbands do not exhibit significant differences between the present and future climates. In contrast to that demonstrated in previous studies, only a very slight northward shift is observed in the baiu region near Tokyo. Our analysis reveals that a considerable meridional shift of the monsoonal front is not expected to occur in the future. The same estimation has been conducted for the period of only June and July, representing

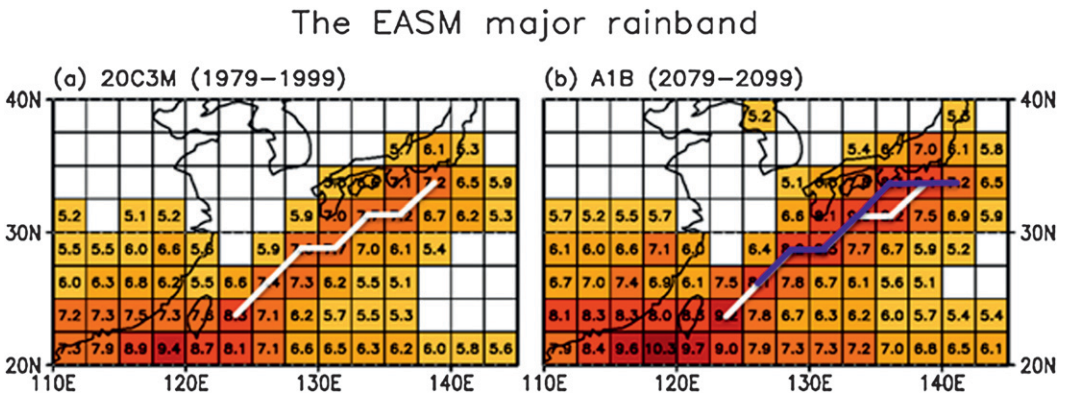

FIG. 7. JJA-mean precipitation (mm day^{-1}) at each grid point for (a) the present-day climate and (b) the future climate. The white line denotes an estimated monsoonal rainband in the good-model composite for present climate conditions; the blue line represents that for the future climate.

baiu season in Japan. The monsoonal rainband exhibits no significant meridional shift (not shown), similar to the above JJA result.

5. Summary and discussion

Future changes in the EASM have been estimated from the six best-performing CMIP3 models. The composite mean rainband over East Asia during the summer season in these models exhibits the characteristic EASM front relatively well with slightly less precipitation over east–central China. In addition, the baiu front is aligned more steeply in the latitudinal direction. The composite analysis results from this strategy differed significantly from the all-member ensemble mean. In addition, moisture flux and temperature fields (and other fields not shown in this paper, such as sea level pressure and upper-level circulation patterns) composited from the good models that are selected solely on the basis of precipitation show more realistic distributions than the 22-model ensemble mean or poor-model ensemble mean, indicating the effectiveness of our approach. Models that poorly simulated the EASM degrade the overall results. A major degradation is the underestimation of the projected increase in precipitation. That is, the all-member ensemble-mean precipitation anticipates an increase of only 5%–10% for the period of 2079–99; however, the corresponding mean precipitation increase rate from the good models, 10%–20%, is twice that rate. In the future, cumulus convective precipitation is expected to increase more strongly (10%–50%) due to an increase in convective instability (not shown) than the precipitation from large-scale condensation.

To estimate important processes for the enhanced precipitation along the monsoon front under the warm climate in a more quantitative manner, a moisture budget equation is analyzed. The individual terms (water content tendency, moisture advection, moisture divergence, precipitation, evaporation, and residual) composing the budget equation exhibit much better correspondence with observations in the good-model ensemble mean than in the poor- or all-model ensemble mean over the EASM region, supporting the robust results from the best-performing models. The poor-model ensemble mean shows the considerable deficiency in simulating moisture flux convergence, in particular moist advection, leading to an unrealistic precipitation structure. In the future climate, the vertically integrated moisture flux convergence $-\nabla \cdot q\mathbf{V}_H$ increases by ~15%, which is mainly attributed to enhanced precipitation over the EASM region (Figs. 3 and 6). The increase by moisture convergence $-q\nabla \cdot \mathbf{V}_H$ is twice greater than that by moist advection $-\mathbf{V}_H \cdot \nabla q$. Of the two contributions of increased water vapor content and convergence by low-level winds, the increase of atmospheric water vapor caused by a ~2.5°–4°C increase in the SST over the vast western Pacific plays a more critical role in the enhanced precipitation in the future climate than a change in the low-level circulation.

In contrast to the apparent meridional shift of the primary location of the future EASM front described in previous studies, the current analysis shows negligible meridional movement in the future. On the other hand, we have analyzed the EASM change for the near future (2020–40) using the same method. Results show overall patterns similar to those during the last two decades of the twenty-first century with only weaker intensity. Precipitation is expected to increase by 5%–10%, cumulus convective precipitation is expected to increase by 5%–15%, and moisture flux is expected to increase by 15%–30%.

The current study suggests that downscaling of the local precipitation changes should be performed with

only climate models that simulate precipitation variability reasonably well. This strategy will lessen the burden on the estimation of regional or local precipitation changes in future climates (Joseph and Nigam 2006).

Acknowledgments. This work was funded by the Korea Meteorological Administration Research and Development Program under Grant CATER 2012–3071. The authors acknowledge the support from the Korea Institute of Science and Technology Information (KISTI).

REFERENCES

Chen, H. P., and J. Q. Sun, 2009: How the ''best'' models project the future precipitation change in China. *Adv. Atmos. Sci.,* **26,** 773–782.

Hsu, P.-C., T. Li, J.-J. Luo, H. Murakami, and A. Kitoh, 2012: Increase of global monsoon area and precipitation under global warming: A robust signal? *Geophys. Res. Lett.,* **39,** L06701, doi:10.1029/2012GL051037.

Joseph, R., and S. Nigam, 2006: ENSO evolution and teleconnection in IPCC's twentieth-century climate simulations: Realistic representation? *J. Climate,* **19,** 4360–4377.

Kanamitsu, M., W. Ebisuzaki, J. Woollen, S.-K. Yang, J. J. Hnilo, M. Fiorino, and G. L. Potter, 2002: NCEP–DOE AMIP-II Reanalysis (R-2). *Bull. Amer. Meteor. Soc.,* **83,** 1631–1643.

Kim, M.-J., J.-H. Shin, H.-S. Lee, and W.-T. Kwon, 2008: An uncertainty assessment of AOGCM and future projection over East Asia. *J. Korean Meteor. Soc.,* **18,** 507–524.

Kimoto, M., 2005: Simulated change of the East Asian circulation under global warming scenario. *Geophys. Res. Lett.,* **32,** L16701, doi:10.1029/2005GL023383.

——, C. Yasutomi, Yokoyama, and S. Emori, 2005: Projected changes in precipitation characteristics around Japan under the global warming. *SOLA,* **1,** 85–88.

Kitoh, A., and T. Uchiyama, 2006: Changes in onset and withdrawal of the East Asian summer rainy season by multi-model global warming experiments. *J. Meteor. Soc. Japan,* **84,** 247–258.

Kripalani, R. H., J.-H. Oh, and H. S. Chaudhari, 2007: Response of the East Asian summer monsoon to doubled atmospheric CO_2: Coupled climate model simulations and projections under IPCC AR4. *Theor. Appl. Climatol.,* **87,** 1–28.

Krishnamurti, T. N., C. M. Kishtawal, Z. Zhang, T. Larow, D. Bachiochi, and E. Willford, 2000: Multimodel ensemble forecasts for weather and seasonal climate. *J. Climate,* **13,** 4196–4216.

Kusunoki, S., and O. Arakawa, 2012: Change in the precipitation intensity of the East Asian summer monsoon projected by CMIP3 models. *Climate Dyn.,* **38,** 2055–2072, doi:10.1007/s00382-011-1234-7.

——, R. Mizuta, and M. Matsueda, 2011: Future changes in the East Asian rain band projected by global atmospheric models with 20-km and 60-km grid size. *Climate Dyn.,* **37,** 2481–2493, doi:10.1007/s00382-011-1000-x.

Li, J. P., Z. W. Wu, Z. H. Jiang, and J. H. He, 2010: Can global warming strengthen the East Asian summer monsoon? *J. Climate,* **23,** 6696–6705.

Lu, R., and Y. Fu, 2010: Intensification of East Asian summer rainfall interannual variability in the twenty-first century simulated by 12 CMIP3 coupled models. *J. Climate,* **23,** 3316–3331.

——, Y. Li, and B. Dong, 2007: East Asian precipitation increase under the global warming. *J. Korean. Meteor. Soc.,* **43,** 267–272.

Min, H.-J., and J.-G. Jhun, 2010: The change in the East Asian summer monsoon simulated by the MIROC3.2 high-resolution coupled model under global warming scenarios. *Asia-Pac. J. Atmos. Sci.,* **46,** 73–88.

Min, S.-K., E.-H. Park, and W.-T. Kwon, 2004: Future projections of East Asian climate change from multi-AOGCM ensembles of IPCC SRES scenario simulations. *J. Meteor. Soc. Japan,* **82,** 1187–1211.

——, S. Legutke, A. Hense, U. Cubasch, W.-T. Kwon, J.-H. Oh, and U. Schlese, 2006: East Asian climate change in the 21st century as simulated by the coupled climate model ECHO-G under IPCC SRES scenarios. *J. Meteor. Soc. Japan,* **84,** 1–26.

Seager, R., N. Naik, and G. A. Vecchi, 2010: Thermodynamic and dynamic mechanisms for large-scale changes in the hydrological cycle in response to global warming. *J. Climate,* **23,** 4651–4668.

Taylor, K. E., 2001: Summarizing multiple aspects of model performance in a single diagram. *J. Geophys. Res.,* **106** (D7), 7183–7192.

Xie, P., and P. A. Arkin, 1997: Global precipitation: A 17-year monthly analysis based on gauge observations, satellite estimates, and numerical model outputs. *Bull. Amer. Meteor. Soc.,* **78,** 2539–2558.

Yoon, J.-H., and T.-C. Chen, 2005: Water vapor budget of the Indian monsoon depression. *Tellus,* **57A,** 770–782.

Yun, K.-S., S.-H. Shin, K.-J. Ha, A. Kitoh, and S. Kusunoki, 2008: East Asian precipitation change in the global warming climate simulated by a 20-km mesh AGCM. *Asia-Pac. J. Atmos. Sci.,* **44,** 233–247.

Zhou, T. J., and R. C. Yu, 2006: Twentieth-century surface air temperature over China and the globe simulated by coupled climate models. *J. Climate,* **19,** 5843–5858.

Copyright of Journal of Climate is the property of American Meteorological Society and its content may not be copied or emailed to multiple sites or posted to a listserv without the copyright holder's express written permission. However, users may print, download, or email articles for individual use.